



ELSEVIER

Available online at www.sciencedirect.com

SCIENCE @ DIRECT®

Journal of Computational Physics 194 (2004) 278–303

JOURNAL OF
COMPUTATIONAL
PHYSICS

www.elsevier.com/locate/jcp

Exact non-reflecting boundary conditions on general domains

David P. Nicholls^{a,*}, Nilima Nigam^b

^a Department of Mathematics, University of Notre Dame, Notre Dame, IN 46556, USA

^b Department of Mathematics and Statistics, McGill University, Montréal, QC, Canada H3A 2K6

Received 21 November 2002; received in revised form 22 September 2003; accepted 22 September 2003

Abstract

The authors present a new method for the realization of exact non-reflecting (transparent) boundary conditions in two dimensional direct scattering problems. This work is an extension of Keller, Givoli, and Grote's work on such conditions which required that the shape of the boundary be quite specific, i.e. circular or elliptical. The condition is enforced via the Dirichlet–Neumann operator (DNO) which, on general boundaries, presents the main difficulty in the method. The implementation is performed by one of two perturbative methods (where the perturbation parameter measures the deformation of the general geometry from a canonical one). A rigorous proof of the analyticity for the DNO with respect to this perturbation parameter is presented. Numerical results show both perturbative methods are fast and accurate, and can enable significant computational savings.

© 2003 Elsevier B.V. All rights reserved.

Keywords: Non-reflecting boundary conditions; Transparent boundary conditions; Acoustic scattering; Electromagnetic scattering; Dirichlet–Neumann operators; Dirichlet-to-Neumann maps; Geometric perturbation methods

1. Introduction

Many problems in science and engineering involve problems posed on domains of infinite extent and, in order to realize a unique solution, one must typically specify the behavior of the solution at infinity. In this paper we focus on a numerical technique for enforcing these conditions *exactly* in the context of two dimensional electromagnetic and acoustic bounded obstacle scattering. In scattering applications the appropriate condition at infinity is the Sommerfeld radiation condition which mandates that, given incoming radiation incident upon a scatterer, the scattered waves must be outgoing [14,49]. Of course, numerical simulations require a truncation of the computational domain to one of *finite* extent. The reduced problem should be well-posed, convenient to implement, and yield accurate approximations to solutions of the original scattering problem. These aims are often conflicting, and much past and current research centers on this issue.

* Corresponding author. Tel.: +574-631-8706; fax: +574-631-6579.

E-mail addresses: nicholls.2@nd.edu (D.P. Nicholls), nigam@math.mcgill.ca (N. Nigam).

A common approach to computational approximations is to introduce an *artificial boundary*, \mathcal{B} , away from the scatterer and enforce a boundary condition there which incorporates information about the far-field behavior of the scattered field (see Fig. 1). A very simple and popular choice of boundary condition on \mathcal{B} is the *natural* (Neumann) boundary condition. Given the exact Dirichlet trace of the scattered wave on \mathcal{B} , one obtains this Neumann boundary condition via the Poincaré–Steklov map. These maps are defined for very general shapes \mathcal{B} , and are *non-local* in nature. It is easily seen that prescribing such boundary conditions leads to a reduced problem which is well-posed. The implementation of such a map, however, poses interesting computational challenges. One possibility is the use of boundary integral equations to obtain this map [34,35]. While this method requires few restrictions on the shape of \mathcal{B} , it necessitates the computation of integrals with singular kernels, and leads (at the discretized level) to unacceptably dense matrices. A more severe drawback to boundary integral methods is the absence of high-order quadrature methods, especially in three dimensions. Finally, boundary integral methods are not effective in time-dependent problems.

On the other hand, if the surface \mathcal{B} is simple then, as we shall see in Section 3, the Dirichlet problem exterior to the artificial boundary can be solved exactly using separation of variables [32]. This can be used to prescribe the Poincaré–Steklov map *exactly* at \mathcal{B} . In the literature featuring this approach, the Poincaré–Steklov map is more commonly referred to as a Dirichlet–Neumann operator (DNO), or as a Dirichlet-to-Neumann (DtN) map [24,37]. This boundary condition coupled with a finite element method (FEM) discretization of the resulting domain of finite extent is the DtN-FE method of Keller and Givoli [22–24,37] and Keller and Grote [28]. We note that the DtN-FE method is not specific to scattering applications and has been generalized to problems in elasticity and time dependent problems [23,27,29,30] (see also the list of references in [24]).

This approach is limited in two ways: The requirement that the artificial boundary be of a quite simple shape (circular or elliptical in two dimensions, and spherical or ellipsoidal in three dimensions) and the non-local nature of the DNO. The latter limitation stems from the non-local nature of the Poincaré–Steklov maps: The discretization of the DNO results in dense sub-matrices being introduced into otherwise sparse linear systems, and degraded accuracy when the DNO is applied to functions of low smoothness (which typically occur in FEM simulations). This concern has been examined by several authors (see Givoli’s survey paper [24]). Indeed, many *local* approximate boundary conditions have been devised, including the perfectly matched layer [4]. However, these local boundary conditions either have stability issues [1,3], or cause spurious reflections into the computational region. A uniformly satisfactory local boundary condition has not been invented and the DtN-FE method, which eliminates these spurious reflections, remains important in applications.

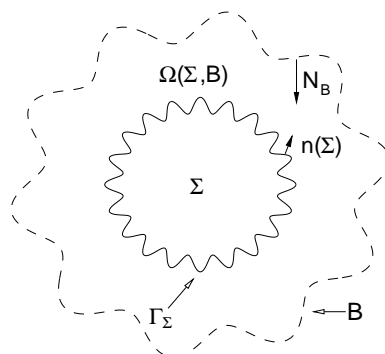


Fig. 1. Depiction of a scatterer, Σ , with boundary Γ_Σ and unit exterior normal $n(\Sigma)$ enclosed within the artificial boundary \mathcal{B} with normal N_B . The region $\Omega(\Sigma, \mathcal{B})$ is the intersection of the exterior of Σ with the interior of \mathcal{B} .

The aim of the current research is to address the geometric limitation of the DtN-FE method: The specific form of the artificial boundary \mathcal{B} required. Our approach is inspired by the work of Milder and Sharp [39–43], Craig and Sulem [17], and Nicholls and Reitich [46–48] on perturbative methods for computation of DNO on domains which are deformations of simple (separable) regions. This work is also very much in the spirit of the perturbative calculations of grating and bounded-obstacle scattering due to Bruno and Reitich [5–12], the first-order calculations of Yeh [53], and the scattering matrix calculations of Givoli [25]. Milder [39–42] and Milder and Sharp [43] devised a numerical method for grating scattering of acoustic and electromagnetic waves which produced, via integral formulas, the scattered field from incident radiation and the DNO at the surface of the scatterer. Assuming that the shape of the scatterer was a small (but general) deformation of a plane they formulated a recursive procedure (denoted the Method of operator expansions (OE), see Section 3.2) for calculating the terms in the Taylor series expansion of the DNO about this canonical geometry. Independently, Craig and Sulem [17] noted that the Hamiltonian for free-surface ideal fluid flows (the water wave problem), due to Zakharov [54], could be rewritten entirely in terms of surface variables with the introduction of a DNO associated with Laplace's equation on the *irregular* domain occupied by the ideal fluid. Using the analyticity properties of the DNO with respect to surface deformations [15,18,45,46,48] they produced recursive OE formulas for the Taylor series of the DNO and conducted several low (fourth and fifth) order calculations. Nicholls and Reitich [46–48] investigated the conditioning properties of the OE and field expansions (FE) [6–8,20] methods for computing the DNO associated with Laplace's equation on irregular domains and, upon identifying their unstable nature at high order, devised a new, stable high order method (termed the method of transformed field expansions (TFE)) which, at the cost of somewhat greater computational complexity, produces highly accurate approximations in a stable fashion.

Our approach expands the DtN-FE method by enlarging the class of allowable artificial boundaries to include perturbations of a simple (separable) surface: A circle in two dimensions and a sphere in three dimensions. This generalization is shown to be fast and accurate, and, in the setting of irregular bounded obstacle scattering, it is demonstrated that this new algorithm can greatly reduce the cost of non-reflecting boundary conditions thereby enabling the simulation of otherwise prohibitive configurations (Note the number of elements required to enclose the star-shaped scatterer with a circle in Fig. 8(a) as opposed to the star-shaped boundary in Fig. 8(b)). Indeed, since ellipses, rectangles, and even the star-shaped domain in Fig. 8(b) (to name just a few) may be approximated by a perturbation of a circle, our framework allows the immediate implementation of artificial boundaries with these useful shapes without recourse to the computation of complicated, numerically unstable basis functions, e.g. Mathieu functions relevant to elliptical geometries [28]. Our approach will also have advantages over methods such as the recent extension of Djellouli et al. [19] of the Bayliss–Turkel non-reflecting boundary conditions to non-circular *convex* artificial boundaries. Not only is our boundary condition *exactly* transparent but it also permits, as Fig. 8(b) illustrates, perturbations which can give rise to *non-convex* artificial boundaries.

The choice of the Poincaré–Steklov map to prescribe the artificial boundary condition is by no means the only one possible. Indeed, there is a vast literature concerning the characterization of solutions to partial differential equations in terms of their boundary traces, using the machinery of pseudodifferential operators (see, e.g., [33,51] for a good introductory exposition). One may use the difference potentials method of [50] to construct artificial boundary conditions (see, e.g., the review article [52] and references therein). In this technique, the computation of a Calderón projection for an arbitrary artificial boundary would typically require the solution of an auxiliary problem on a (larger) regular domain containing the scatterer and the artificial boundary.

The organization of the paper is as follows: In Section 2 we discuss the governing equations of direct scattering in two dimensions and the FEM for numerical simulations of such problems when coupled with non-reflecting boundary conditions. In Section 3 we discuss the DNO on perturbed geometries, methods for its perturbative calculation, and a rigorous analyticity result for DNO. We conclude with Section 4 where

numerical simulations are presented which illustrate the speed, accuracy, and advantages in complexity of our new algorithm.

2. Governing equations and the numerical method

In two dimensions Helmholtz’s equation governs the amplitude of a time-harmonic plane wave scattered by a bounded object. In this section we show how the problem on an infinite domain together with the radiation boundary condition can be reformulated as a problem on a finite domain with an exact boundary condition at the outer boundary. We then show how the FEM can be used to discretize this problem.

2.1. Electromagnetic and acoustic scattering in two dimensions

The total field, v_T , associated with a two dimensional time-periodic electromagnetic or acoustic plane wave incident upon a bounded, perfectly conducting (impenetrable) object $\Sigma \subset \mathbf{R}^2$ satisfies Helmholtz’s equation

$$\Delta v_T + k^2 v_T = 0 \quad \text{in } \mathbf{R}^2 \setminus \bar{\Sigma}, \tag{1}$$

where k is given by the wavenumber of the incident radiation, coupled with either a Dirichlet or Neumann condition at the boundary of the scatterer, $\partial\Sigma = \Gamma_\Sigma$ [14,49]. The reflected field $v_r = v$ and incident field v_i also satisfy Helmholtz’s equation (1). The final condition necessary for a unique solution is the Sommerfeld radiation condition which states that reflected waves be outgoing. Gathering these conditions we find, in the Neumann case, that the reflected field must satisfy

$$\Delta v + k^2 v = 0 \quad \text{in } \mathbf{R}^2 \setminus \bar{\Sigma}, \tag{2a}$$

$$\partial_{n(\Sigma)} v = -\partial_{n(\Sigma)} v_i \quad \text{at } \Gamma_\Sigma, \tag{2b}$$

$$\lim_{r \rightarrow \infty} r^{1/2} (\partial_r v - i k v) = 0, \tag{2c}$$

where $n(\Sigma)$ is the unit normal pointing exterior to Σ , see Fig. 1. A considerable challenge to numerical simulation of solutions of (2) is the infinite nature of the domain coupled with the faithful enforcement of the Sommerfeld radiation condition (2c).

A common approach to the numerical solution of (2) is to introduce an artificial boundary \mathcal{B} properly enclosing Σ , and then to discretize the annular domain between them, $\Omega(\Sigma, \mathcal{B})$. More precisely, we discretize the intersection of $\mathbf{R}^2 \setminus \bar{\Sigma}$ and the interior of \mathcal{B} , see Fig. 1. The key consideration in this method is the boundary condition which is enforced at \mathcal{B} . One way to enforce the Sommerfeld radiation condition *exactly* is via a DNO, also known in the literature as a Poincaré–Steklov or DtN map, which maps Dirichlet data ξ at the boundary \mathcal{B} to Neumann data at that boundary,

$$G(\mathcal{B})\xi = \nabla w|_{\mathcal{B}} \cdot N_{\mathcal{B}} \tag{3}$$

(note that $N_{\mathcal{B}}$ is not necessarily a unit vector), where w solves

$$\Delta w + k^2 w = 0 \quad \text{in exterior of } \mathcal{B}, \tag{4a}$$

$$w = \xi \quad \text{at } \mathcal{B}, \tag{4b}$$

$$\lim_{r \rightarrow \infty} r^{1/2}(\partial_r w - ikw) = 0, \quad (4c)$$

and the normal $N_{\mathcal{B}}$ points toward Σ . Now (2) may be equivalently stated as

$$\Delta v + k^2 v = 0 \quad \text{in } \Omega(\Sigma, \mathcal{B}), \quad (5a)$$

$$\partial_{n(\Sigma)} v = -\partial_{n(\Sigma)} v_i \quad \text{at } \Gamma_{\Sigma}, \quad (5b)$$

$$\nabla v \cdot N_{\mathcal{B}} = G(\mathcal{B})v \quad \text{at } \mathcal{B}. \quad (5c)$$

Of course the utility of this method depends heavily upon the ease and accuracy with which one can compute the DNO associated with the artificial boundary; this issue is discussed in depth in Section 3.

2.2. Finite element formulation

For simplicity of presentation we shall from now on consider the Neumann problem (5); the Dirichlet problem requires only straightforward modifications. The weak form of (5) is, for any test function $\varphi \in H^1(\Omega(\Sigma, \mathcal{B}))$,

$$a(v, \varphi) = f(\varphi), \quad (6)$$

where

$$a(v, \varphi) = - \int_{\Omega(\Sigma, \mathcal{B})} \nabla v \cdot \nabla \varphi \, dV + k^2 \int_{\Omega(\Sigma, \mathcal{B})} v \varphi \, dV - \int_{\mathcal{B}} \frac{G(\mathcal{B})v}{|N_{\mathcal{B}}|} \varphi \, dS,$$

$$f(\varphi) = - \int_{\Gamma_{\Sigma}} (\partial_{n(\Sigma)} v_i) \varphi \, dS.$$

The finite element discretization [36] of (6) begins by triangulating $\Omega(\Sigma, \mathcal{B})$,

$$\Omega(\Sigma, \mathcal{B}) = \bigcup_{j=1}^{N_t} \mathcal{T}_j,$$

which produces the vertex nodes v_j , $j = 1, \dots, N_p$. We define

$$h = \max_{1 \leq j \leq N_t} \text{diam}(\mathcal{T}_j), \quad (7)$$

a triangular mesh parameter. In the case of the piecewise linear FEM let us define

$$V_h = \{v | v \text{ is continuous on } \Omega(\Sigma, \mathcal{B}), v|_{\mathcal{T}_j} \text{ is linear}\},$$

which is spanned by $\varphi_1, \dots, \varphi_{N_p}$ where φ_j is a linear function such that $\varphi_j(v_k) = \delta_{j,k}$, the Kronecker delta. The Galerkin FEM seeks a solution $\tilde{v} \in V_h$,

$$\tilde{v} = \sum_{j=1}^{N_p} v_j \varphi_j,$$

such that

$$a(\tilde{v}, \varphi) = f(\varphi), \quad \forall \varphi \in V_h.$$

This is equivalent to the linear system

$$(-K + k^2M + Q)\vec{v} = \vec{f}, \tag{8}$$

where $\vec{v}_j = v_j$,

$$K_{j,k} = \int_{\Omega(\Sigma, \mathcal{B})} \nabla \varphi_j \cdot \nabla \varphi_k \, dV, \tag{9a}$$

$$M_{j,k} = \int_{\Omega(\Sigma, \mathcal{B})} \varphi_j \varphi_k \, dV, \tag{9b}$$

$$Q_{j,k} = - \int_{\mathcal{B}} \frac{G(\mathcal{B})\varphi_j}{|N_{\mathcal{B}}|} \varphi_k \, dS, \tag{9c}$$

$$\vec{f}_k = - \int_{\Gamma_{\Sigma}} (\partial_{n(\Sigma)} v_i) \varphi_k \, dS. \tag{9d}$$

The matrices K (stiffness) and M (mass), and vector \vec{f} can all be calculated in a standard manner [36]; the only calculation left to be described is that of Q . For arbitrary \mathcal{B} this is quite difficult, but if \mathcal{B} is of a specific (but quite general) type, e.g. a deformation of a circle, then, as we shall see in Sections 3.1 and 3.2, it can be accomplished simply, quickly, and accurately via perturbation techniques.

3. The Dirichlet–Neumann operator

In order for the reformulation of the scattering problem on a bounded domain (5) to be useful, one must be able to enforce (5c), i.e. one must be able to compute the DNO, $G(\mathcal{B})$, which allows one to approximate the matrix Q in (8). The approach investigated by Han and Wu [32] and Keller and Givoli [37] considers an artificial boundary \mathcal{B} of circular type, i.e.

$$\mathcal{B} = \{r = a\}.$$

In this case one can write the *exact* solution of (4) as

$$w(r, \theta) = \sum_{p=-\infty}^{\infty} \frac{H_p^{(1)}(kr)}{H_p^{(1)}(ka)} \hat{\xi}_p e^{ip\theta},$$

where $\xi(\theta) = \sum_{p=-\infty}^{\infty} \hat{\xi}_p e^{ip\theta}$, and $H_p^{(1)}$ is the p th Hankel function of the first kind (or Bessel function of the third kind). From this and (3) we can write the DNO as

$$G(r = a)\xi = - \sum_{p=-\infty}^{\infty} k \frac{d_z H_p^{(1)}(ka)}{H_p^{(1)}(ka)} \hat{\xi}_p e^{ip\theta} = -k \frac{d_z H_D^{(1)}(ka)}{H_D^{(1)}(ka)} \xi, \tag{10}$$

where d_z denotes differentiation of the Hankel function with respect to its argument. Note that this formula defines the Fourier multiplier

$$\frac{d_z H_D^{(1)}(ka)}{H_D^{(1)}(ka)},$$

where $D = -i\partial_x$.

While this approach has been useful in applications [22,26–30,37] and has been extended to boundaries of elliptic shape, there are many scatterers which are not efficiently enclosed by either a circle or an ellipse (e.g. star-like domains, see Fig. 8) resulting in many unnecessary elements far from Σ which must be included in the computation.

We can significantly enlarge the class of artificial boundaries if we allow a perturbation of a circle, say

$$\mathcal{B} = \{r = a + g(\theta)\}.$$

If the size of the deformation, g , from the circular separable geometry, $r = a$, is small then a perturbative approach is natural and will be highly efficient and accurate. In fact, if we now specify $g(\theta) = \delta f(\theta)$, then, as we shall prove in Section 3.3, the DNO is *analytic* with respect to the perturbation parameter δ (Theorem 1), i.e. we can write the Taylor series

$$G(\delta f)\xi = \sum_{n=0}^{\infty} (G_n(f)\xi)\delta^n, \tag{11}$$

which converges in a strong sense made precise in the following result.

Theorem 1. *Given an integer $s \geq 0$, if $f \in C^{s+2}([0, 2\pi])$ then the series (11) converges strongly as an operator from $H^{s+3/2}([0, 2\pi])$ to $H^{s+1/2}([0, 2\pi])$. In other words there exists a constant K_1 such that*

$$\|G_n(f)\xi\|_{H^{s+1/2}} \leq K_1 \|\xi\|_{H^{s+3/2}} B^n$$

for any $B > C\|f\|_{C^{s+2}}$.

Furthermore, it can be shown (and will prove to be very useful in Section 4) that the DNO can be analytically continued beyond the disk of convergence guaranteed by Theorem 1. Following [48] we investigate the domain of analyticity of the DNO by fixing $f(\theta)$ and examining

$$G(\varepsilon f)$$

which, Theorem 2 will show, is analytic for all $\varepsilon \in \mathbf{R}$ as long as $|\varepsilon\|f\|_{L^\infty}| < a$, i.e. $\varepsilon \in (-a/\|f\|_{L^\infty}, a/\|f\|_{L^\infty})$. Consider $\varepsilon_0 \in (-a/\|f\|_{L^\infty}, a/\|f\|_{L^\infty})$ and let

$$f_0 = \varepsilon_0 f, \quad \delta = \varepsilon - \varepsilon_0.$$

Then

$$G(\varepsilon f) = G(f_0 + \delta f)$$

and the problem of determining the domain of analyticity of the DNO reduces to establishing analyticity in δ at $\delta = 0$, i.e. the convergence of the series

$$G(f_0 + \delta f)\xi = \sum_{n=0}^{\infty} (G_n(f_0, f)\xi)\delta^n. \tag{12}$$

We now state, without proof (please see [48]), the following theorem.

Theorem 2. *Given an integer $s \geq 0$, if $f_0, f \in C^{s+2}([0, 2\pi])$ then the series (12) converges strongly as an operator from $H^{s+3/2}([0, 2\pi])$ to $H^{s+1/2}([0, 2\pi])$.*

The focus of the next two subsections is the formulation of two methods for the numerical approximation of the G_n in (11). The final subsection is dedicated to the rigorous proof of Theorem 1.

3.1. Field expansions

The method of FE for computing the DNO [6–8,20,46–48] is based upon the fact that both the DNO and the field are analytic with respect to boundary variations, parameterized by δ (Theorems 1 and 3, respectively). With this in mind we expand the field w in powers of δ ,

$$w(r, \theta, \delta) = \sum_{n=0}^{\infty} w_n(r, \theta) \delta^n, \tag{13}$$

and insert this into the defining Helmholtz problem (4) with $\mathcal{B} = \{r = a + \delta f\}$. By equating like powers of δ we find that the w_n must satisfy

$$\Delta w_n(r, \theta) + k^2 w_n(r, \theta) = 0 \quad r > a, \tag{14a}$$

$$w_n(a, \theta) = \delta_{n,0} \xi(\theta) - \sum_{l=0}^{n-1} \partial_r^{n-l} w_l(a, \theta) \frac{f^{n-l}}{(n-l)!}, \tag{14b}$$

$$\lim_{r \rightarrow \infty} r^{1/2} (\partial_r w_n - i k w_n) = 0, \tag{14c}$$

where $\delta_{n,p}$ is the Kronecker delta. Noting that

$$w_n(r, \theta) = \sum_{p=-\infty}^{\infty} a_{n,p} H_p^{(1)}(kr) e^{ip\theta}, \tag{15}$$

satisfies Eqs. (14a) and (14c), we can use (14b) to derive recursive formulas for the Fourier coefficients $a_{n,p}$:

$$a_{n,p} = \delta_{n,0} \frac{\hat{\xi}_p}{H_p^{(1)}(ka)} - \sum_{l=0}^{n-1} \sum_{q=-\infty}^{\infty} C_{n-l,p-q} \frac{d_z^{n-l} H_q^{(1)}(ka)}{H_p^{(1)}(ka)} a_{l,q}$$

where the $C_{l,p}$ are defined by

$$\frac{k^l f(\theta)^l}{l!} = \sum_{p=-\infty}^{\infty} C_{l,p} e^{ip\theta}.$$

With the $a_{n,p}$ in hand we can now compute the n th term in the expansion of the DNO. Recalling Eqs. (3), (13) and (15) we note that

$$\begin{aligned} G(\delta f) \xi &= \nabla w(a + \delta f(\theta), \theta) \cdot N_{\delta f} \\ &= \sum_{n=0}^{\infty} \sum_{p=-\infty}^{\infty} \left[-k(a + \delta f) d_z H_p^{(1)}(k(a + \delta f)) + \frac{\delta \partial_{\theta} f}{(a + \delta f)} (ip) H_p^{(1)}(k(a + \delta f)) \right] a_{n,p} e^{ip\theta} \delta^n, \end{aligned}$$

where $N_{\delta f} = (-(a + \delta f), \delta \partial_{\theta} f)$. If we multiply by $(a + \delta f)$ (to remove quotients involving δ terms) and expand the DNO in powers of δ we discover the following recursion for $G_n(f)$

$$\begin{aligned}
 G_n(f)\xi &= -ka \sum_{l=0}^n \sum_{p=-\infty}^{\infty} a_{l,p} \frac{(kf)^{n-l}}{(n-l)!} d_z^{n+1-l} H_p^{(1)}(ka) e^{ip\theta} - \frac{f}{a} G_{n-1}(f)\xi \\
 &\quad - 2kf \sum_{l=0}^{n-1} \sum_{p=-\infty}^{\infty} a_{l,p} \frac{(kf)^{n-1-l}}{(n-1-l)!} d_z^{n-l} H_p^{(1)}(ka) e^{ip\theta} - \frac{k}{a} f^2 \sum_{l=0}^{n-2} \sum_{p=-\infty}^{\infty} a_{l,p} \frac{(kf)^{n-2-l}}{(n-2-l)!} \\
 &\quad \times d_z^{n-1-l} H_p^{(1)}(ka) e^{ip\theta} + \frac{1}{a} (\partial_\theta f) \sum_{l=0}^{n-1} \sum_{p=-\infty}^{\infty} a_{l,p} \frac{(kf)^{n-1-l}}{(n-1-l)!} d_z^{n-1-l} H_p^{(1)}(ka) (ip) e^{ip\theta}. \tag{16}
 \end{aligned}$$

3.2. Operator expansions

In contrast to the FE method outlined above, the method of OE [17,39–43,46–48] computes *directly* the terms G_n in the perturbation series for the DNO (11). Again recalling the defining Helmholtz problem (4) we note that a solution of (4a) and (4c) is

$$w_p(r, \theta) = H_p^{(1)}(kr) e^{ip\theta}.$$

Now

$$w_p(a + \delta f, \theta) = H_p^{(1)}(k(a + \delta f)) e^{ip\theta}$$

so that from the definition of the DNO, (3),

$$G(\delta f) \left[H_p^{(1)}(k(a + \delta f)) e^{ip\theta} \right] = -(a + \delta f) \partial_r \left(H_p^{(1)}(kr) e^{ip\theta} \right) \Big|_{r=a+\delta f} + \frac{\delta \partial_\theta f}{a + \delta f} \partial_\theta \left(H_p^{(1)}(kr) e^{ip\theta} \right) \Big|_{r=a+\delta f},$$

that is

$$G(\delta f) \left[H_p^{(1)}(k(a + \delta f)) e^{ip\theta} \right] = -k(a + \delta f) d_z H_p^{(1)}(k(a + \delta f)) e^{ip\theta} + \frac{\delta \partial_\theta f}{a + \delta f} (ip) H_p^{(1)}(k(a + \delta f)) e^{ip\theta}. \tag{17}$$

Thus, after multiplying (17) through by $(a + \delta f)$, we expand the result in a series in δ and, equating like powers, obtain

$$\begin{aligned}
 G_n(f) e^{ip\theta} &= -ak \frac{(kf)^n}{n!} \frac{d_z^{n+1} H_p^{(1)}(ka)}{H_p^{(1)}(ka)} e^{ip\theta} - 2fk \frac{(kf)^{n-1}}{(n-1)!} \frac{d_z^n H_p^{(1)}(ka)}{H_p^{(1)}(ka)} e^{ip\theta} - \frac{f^2 k}{a} \frac{(kf)^{n-2}}{(n-2)!} \frac{d_z^{n-1} H_p^{(1)}(ka)}{H_p^{(1)}(ka)} e^{ip\theta} \\
 &\quad + \frac{\partial_\theta f}{a} \frac{(kf)^{n-1}}{(n-1)!} \frac{d_z^{n-1} H_p^{(1)}(ka)}{H_p^{(1)}(ka)} (ip) e^{ip\theta} - \sum_{l=0}^{n-1} G_l(f) \left[\frac{(kf)^{n-l}}{(n-l)!} \frac{d_z^{n-l} H_p^{(1)}(ka)}{H_p^{(1)}(ka)} e^{ip\theta} \right] \\
 &\quad - \frac{f}{a} \sum_{l=0}^{n-1} G_l(f) \left[\frac{(kf)^{n-1-l}}{(n-1-l)!} \frac{d_z^{n-1-l} H_p^{(1)}(ka)}{H_p^{(1)}(ka)} e^{ip\theta} \right].
 \end{aligned}$$

Recognizing $\xi(\theta)$ as a sum of Fourier modes $e^{ip\theta}$, and using the self-adjoint nature of the operators $G_l(f)$ and $d_z^l H_D^{(1)}(ka)$, we obtain

$$\begin{aligned}
 G_n(f)\xi &= -ak \frac{d_z^{n+1}H_D^{(1)}(ka)}{H_D^{(1)}(ka)} \frac{(kf)^n}{n!} \xi - 2k \frac{d_z^n H_D^{(1)}(ka)}{H_D^{(1)}(ka)} f \frac{(kf)^{n-1}}{(n-1)!} \xi - \frac{k}{a} \frac{d_z^{n-1}H_D^{(1)}(ka)}{H_D^{(1)}(ka)} f^2 \frac{(kf)^{n-2}}{(n-2)!} \xi \\
 &\quad - \frac{1}{a} \frac{d_z^{n-1}H_D^{(1)}(ka)}{H_D^{(1)}(ka)} D(Df) \frac{(kf)^{n-1}}{(n-1)!} \xi - \sum_{l=0}^{n-1} \frac{d_z^{n-l}H_D^{(1)}(ka)}{H_D^{(1)}(ka)} \frac{(kf)^{n-l}}{(n-l)!} G_l(f)\xi \\
 &\quad - \frac{1}{a} \sum_{l=0}^{n-1} \frac{d_z^{n-1-l}H_D^{(1)}(ka)}{H_D^{(1)}(ka)} \frac{(kf)^{n-1-l}}{(n-1-l)!} G_l(f)[f\xi].
 \end{aligned} \tag{18}$$

3.3. Analyticity

In the case of Laplace’s equation ($k = 0$) the analyticity properties of the DNO have been well studied in Cartesian coordinates. From the work of Calderón [13] and Coifman and Meyer [15] the analyticity of the DNO with respect to δ can be deduced for domains with upper boundary shaped by a Lipschitz curve. This was extended by Craig et al. [18] and Craig and Nicholls [16] to the case of three and n dimensions respectively for domains with C^1 upper boundaries. In all of this work the analyticity properties were deduced from an implicit integral equation formula for the DNO coupled with delicate estimates on singular integral operators.

In contrast, and with stable high-order computations in mind, Nicholls and Reitich [46] established the analyticity of the DNO *directly* using a transformed set of recursions. We shall use this method of TFE for the analyticity proof of the DNO due to its direct nature. It should be noted that while the OE and FE recursions cannot be used for a verification of the analyticity of the DNO, they are, as we shall see in Section 4, highly accurate and stable over a large range of physically relevant deformations f and sizes δ .

We begin our proof by introducing a second artificial boundary at $\{r = b\}$, where $b > a + \delta|f|_{L^\infty}$, and a transparent boundary condition at that boundary, $\partial_r w = Tw$, where

$$T = k \frac{d_z H_D^{(1)}(kb)}{H_D^{(1)}(kb)}.$$

This allows us to state the DNO problem, (4), equivalently on the bounded domain $\Omega(a + \delta f, b)$ as

$$\Delta w + k^2 w = 0 \quad \text{in } \Omega(a + \delta f, b), \tag{19a}$$

$$w = \xi \quad \text{at } r = a + \delta f, \tag{19b}$$

$$\partial_r w - Tw = 0 \quad \text{at } r = b. \tag{19c}$$

Following Nicholls and Reitich [46] we introduce the change of variables

$$r' = \frac{(a - b)r + \delta b f(\theta)}{a - b + \delta f(\theta)},$$

$$\theta' = \theta,$$

which maps the domain $\Omega(a + \delta f, b)$ to the annulus $\Omega_{a,b} = \Omega(a, b)$. The change of variables transforms w into:

$$u(r', \theta', \delta) = w(((a - b + \delta f(\theta'))r' - \delta b f(\theta')) / (a - b), \theta'),$$

and (19) into

$$\Delta'u + k^2u = F(r', \theta', \delta) \quad \text{in } \Omega_{a,b}, \tag{20a}$$

$$u(a, \theta', \delta) = \zeta(\theta'), \tag{20b}$$

$$\partial_{r'}u(b, \theta', \delta) - Tu(b, \theta', \delta) = h(\theta'), \tag{20c}$$

where

$$F = \frac{1}{(a-b)^2} [\partial_{r'}F^{(1)} + \partial_{\theta'}F^{(2)} + F^{(3)}],$$

$$\begin{aligned} F^{(1)} = & -(\delta f)(r')^2\partial_{r'}u + (a-b)b(\delta f)r'\partial_{r'}u - (a-b)(\delta f)(r')^2\partial_{r'}u - (\delta f)^2(r')^2\partial_{r'}u + b(\delta f)^2r'\partial_{r'}u \\ & + (a-b)b(\delta f)r'\partial_{r'}u + b(\delta f)^2r'\partial_{r'}u - b^2(\delta f)^2\partial_{r'}u - (\delta\delta_{\theta'}f)^2(b-r')^2\partial_{r'}u \\ & - (\delta\delta_{\theta'}f)(a-b)(b-r')\partial_{\theta'}u - (\delta\delta_{\theta'}f)(\delta f)(b-r')\partial_{\theta'}u, \end{aligned}$$

$$F^{(2)} = -(\delta\delta_{\theta'}f)(a-b)(b-r')\partial_{r'}u - (\delta f)\partial_{\theta'}u - (\delta f)(\delta\delta_{\theta'}f)(b-r')\partial_{r'}u - (a-b)(\delta f)\partial_{\theta'}u - (\delta f)^2\partial_{\theta'}u,$$

$$\begin{aligned} F^{(3)} = & (\delta\delta_{\theta'}f)^2(b-r')\partial_{r'}u + (\delta\delta_{\theta'}f)(a-b)\partial_{\theta'}u + (\delta\delta_{\theta'}f)(\delta f)\partial_{\theta'}u - 2k^2(\delta f)(a-b)u - k^2(\delta f)^2u \\ & + (\delta f)r'\partial_{r'}u - (a-b)b(\delta f)\partial_{r'}u + (a-b)(\delta f)r'\partial_{r'}u + (\delta f)^2r'\partial_{r'}u - b(\delta f)^2\partial_{r'}u, \end{aligned}$$

and

$$h = \delta \frac{f}{a-b} Tu.$$

Upon dropping the primes, in these new coordinates the DNO becomes

$$(a-b+\delta f)(a+\delta f)G(\delta f)\zeta = -(a-b) \left[(a+\delta f)^2 + (\delta\delta_{\theta}f)^2 \right] \partial_r u(a, \theta) + (a-b+\delta f)(\delta\delta_{\theta}f)\partial_{\theta}u(a, \theta).$$

We expand

$$u(r, \theta, \delta) = \sum_{n=0}^{\infty} u_n(r, \theta)\delta^n,$$

and derive the following equations for u_n

$$\Delta u_n + k^2u_n = (1 - \delta_{n,0})F_n(r, \theta) \quad \text{in } \Omega_{a,b}, \tag{21a}$$

$$u_n(a, \theta) = \delta_{n,0}\zeta(\theta), \tag{21b}$$

$$\partial_r u(b, \theta) - Tu(b, \theta) = (1 - \delta_{n,0})h_n(\theta), \tag{21c}$$

where

$$F_n = \frac{1}{(a-b)^2} [\partial_r F_n^{(1)} + \partial_{\theta} F_n^{(2)} + F_n^{(3)}], \tag{22}$$

$$F_n^{(1)} = -fr^2\partial_r u_{n-1} + (a-b)bfr\partial_r u_{n-1} - (a-b)fr^2\partial_r u_{n-1} - f^2r^2\partial_r u_{n-2} + bf^2r\partial_r u_{n-2} + (a-b)bfr\partial_r u_{n-1} + bf^2r\partial_r u_{n-2} - b^2f^2\partial_r u_{n-2} - (\partial_\theta f)^2(b-r)^2\partial_r u_{n-2} - (\partial_\theta f)(a-b)(b-r)\partial_\theta u_{n-1} - (\partial_\theta f)f(b-r)\partial_\theta u_{n-2},$$

$$F_n^{(2)} = -(\partial_\theta f)(a-b)(b-r)\partial_r u_{n-1} - f\partial_\theta u_{n-1} - f(\partial_\theta f)(b-r)\partial_r u_{n-2} - (a-b)f\partial_\theta u_{n-1} - f^2\partial_\theta u_{n-2},$$

$$F_n^{(3)} = (\partial_\theta f)^2(b-r)\partial_r u_{n-2} + (\partial_\theta f)(a-b)\partial_\theta u_{n-1} + (\partial_\theta f)f\partial_\theta u_{n-2} - 2k^2f(a-b)u_{n-1} - k^2f^2u_{n-2} + fr\partial_r u_{n-1} - (a-b)bfr\partial_r u_{n-1} + (a-b)bfr\partial_r u_{n-1} + f^2r\partial_r u_{n-2} - bf^2\partial_r u_{n-2},$$

and

$$h_n = \frac{f}{a-b}Tu_{n-1}.$$

Finally, the n th term in the expansion of the DNO, (11), can be expressed as

$$G_n(f)\xi = \frac{1}{a(a-b)} \left[-(a-b)a^2\partial_r u_n(a, \theta) - 2a(a-b)f\partial_r u_{n-1}(a, \theta) - (a-b)(f^2 + (\partial_\theta f)^2)\partial_r u_{n-2}(a, \theta) + (a-b)(\partial_\theta f)\partial_\theta u_{n-1}(a, \theta) + f(\partial_\theta f)\partial_\theta u_{n-2}(a, \theta) - (2a-b)fG_{n-1}(f)\xi - f^2G_{n-2}(f)\xi \right]. \tag{23}$$

To estimate the functions u_n we use the following inequalities [46]: For integer $s \geq 0$ and arbitrary $\varepsilon > 0$,

$$\|fu\|_{H^s} \leq M(d, s)\|f\|_{C^s}\|u\|_{H^s},$$

$$\|g\mu\|_{H^{s+1/2}} \leq M(d, s)\|g\|_{C^{s+1/2+\varepsilon}}\|\mu\|_{H^{s+1/2}},$$

if $f \in C^s([0, 2\pi])$, $u \in H^s(\Omega_{a,b})$, $g \in C^{s+1/2+\varepsilon}([0, 2\pi])$, $\mu \in H^{s+1/2}([0, 2\pi])$, and $M(d, s)$ is a constant depending on d and s . Our main result is

Theorem 3. *Given an integer $s \geq 0$, if $f \in C^{s+2}([0, 2\pi])$ and $\xi \in H^{s+3/2}([0, 2\pi])$ there exist constants C_0 and K_0 and a unique solution of (20) such that*

$$\|u_n\|_{H^{s+2}} \leq K_0\|\xi\|_{H^{s+3/2}}B^n \tag{24}$$

for any $B > 2K_0C_0\|f\|_{C^{s+2}}$.

Clearly, once we have established Theorem 3, the analyticity result for the DNO (Theorem 1) follows immediately from Eqs. (23) and (24). The proof of Theorem 3 proceeds by applying an elliptic estimate (Lemma 4) to (21) and then using a recursive lemma (Lemma 5) to obtain the desired result. The elliptic estimate involves the DNO at $\{r = b\}$ but is otherwise standard [21,31,38].

Lemma 4. *For any integer $s \geq 0$, there exists a constant K_0 such that for any $F \in H^{s-1}$, $\xi \in H^{s+1/2}$, $h \in H^{s-1/2}$, the solution of*

$$\Delta w(r, \theta) + k^2w(r, \theta) = F(r, \theta) \quad \text{in } \Omega_{a,b}, \tag{25a}$$

$$w(a, \theta) = \xi(\theta), \tag{25b}$$

$$\partial_r w(b, \theta) - Tw(b, \theta) = h(\theta), \tag{25c}$$

$$w(r, \theta + 2m\pi) = w(r, \theta) \quad \forall m \in \mathbf{Z} \tag{25d}$$

satisfies

$$\|w\|_{H^{s+1}} \leq K_0 [\|F\|_{H^{s-1}} + \|\xi\|_{H^{s+1/2}} + \|h\|_{H^{s-1/2}}]. \tag{26}$$

Proof. As we have mentioned, the proof is standard, but we give the argument in the case $s = 0$ to illustrate the influence of the DNO. We begin by setting $v = w - \Xi$ where

$$\Xi(r, \theta) = \sum_{p=-\infty}^{\infty} \hat{\xi}_p \frac{H_p^{(1)}(kr)}{H_p^{(1)}(ka)} e^{ip\theta}.$$

Note that Ξ solves

$$\Delta \Xi(r, \theta) + k^2 \Xi(r, \theta) = 0 \quad \text{in } \Omega_{a,b},$$

$$\Xi(a, \theta) = \xi(\theta),$$

$$\partial_r \Xi(b, \theta) - T \Xi(b, \theta) = 0,$$

$$\Xi(r, \theta + 2m\pi) = \Xi(r, \theta) \quad \forall m \in \mathbf{Z},$$

so that v satisfies

$$\Delta v(r, \theta) + k^2 v(r, \theta) = F(r, \theta) \quad \text{in } \Omega_{a,b}, \tag{27a}$$

$$v(a, \theta) = 0, \tag{27b}$$

$$\partial_r v(b, \theta) - Tv(b, \theta) = h(\theta), \tag{27c}$$

$$v(r, \theta + 2m\pi) = v(r, \theta) \quad \forall m \in \mathbf{Z}. \tag{27d}$$

Recalling that $H^1(\Omega_{a,b})$ can be defined by the norm:

$$\|w\|_{H^1(\Omega_{a,b})}^2 = \sum_{p=-\infty}^{\infty} \int_a^b r \left(\langle p \rangle^2 |\hat{w}_p(y)|^2 + |\partial_y \hat{w}_p(y)|^2 \right) dr,$$

where

$$\langle p \rangle = \sqrt{1 + p^2},$$

it can be shown, using the asymptotic properties of the Hankel function, that

$$\|w\|_{H^1} \leq \|v\|_{H^1} + \|\Xi\|_{H^1} \leq \|v\|_{H^1} + C_a \|\xi\|_{H^{1/2}}.$$

Using Poincaré’s inequality and the fact that v is zero at $r = a$, we note that

$$\|v\|_{H^1}^2 \leq C_P \int_{\Omega_{a,b}} |\nabla v|^2 dV = C_P \|v\|_{H_0^1}^2,$$

and use the latter as our norm. Multiplying (27a) by \bar{v} , and integrating by parts yields

$$\int_{\Omega_{a,b}} |\nabla v|^2 dV - \int_{\Gamma_b} \bar{v}_b T v_b d\theta = k^2 \int_{\Omega_{a,b}} |v|^2 dV - \int_{\Omega_{a,b}} \bar{v} F dV + \int_{\Gamma_b} \bar{v}_b h d\theta,$$

where v_b is v evaluated at Γ_b . We note that

$$\hat{T}(p) = k \frac{d_z H_p^{(1)}(kb)}{H_p^{(1)}(kb)} = -\frac{\langle p \rangle}{kb} + \hat{R}(p),$$

where the asymptotic behavior of $H_p^{(1)}$ gives

$$\left| \hat{R}(p) \right| = \left| \hat{T}(p) + \frac{\langle p \rangle}{kb} \right| \leq C.$$

Thus, we can write

$$\int_{\Omega_{a,b}} |\nabla v|^2 dV + \int_{\Gamma_b} \bar{v}_b \frac{\langle D \rangle}{kb} v_b d\theta = k^2 \int_{\Omega_{a,b}} |v|^2 dV - \int_{\Omega_{a,b}} \bar{v} F dV + \int_{\Gamma_b} \bar{v}_b h d\theta + \int_{\Gamma_b} \bar{v}_b R v_b d\theta. \tag{28}$$

Since

$$\int_{\Omega_{a,b}} |F \bar{v}| dV \leq \|F\|_{H^{-1}} \|v\|_{H_0^1} \leq \frac{1}{2\alpha} \|F\|_{H^{-1}}^2 + \frac{\alpha}{2} \|v\|_{H_0^1}^2,$$

for $F \in H^{-1}(\Omega_{a,b})$ and $v \in H_0^1(\Omega_{a,b})$, and

$$\int_{\Gamma_b} |h \bar{v}_b| d\theta \leq \|h\|_{H^{-1/2}} \|v_b\|_{H^{1/2}} \leq \frac{1}{2\alpha} \|h\|_{H^{-1/2}}^2 + \frac{\alpha}{2} \|v_b\|_{H^{1/2}}^2,$$

for $h \in H^{-1/2}([0, 2\pi])$ and $v_b \in H^{1/2}([0, 2\pi])$, we can use (28) to deduce that

$$\|v\|_{H_0^1}^2 + \int_{\Gamma_b} \bar{v}_b \frac{\langle D \rangle}{kb} v_b d\theta \leq k^2 \|v\|_{L^2}^2 + \int_{\Gamma_b} |\bar{v}_b R v_b| d\theta + \frac{\alpha}{2} \left(\|v\|_{H_0^1}^2 + \|v_b\|_{H^{1/2}}^2 \right) + \frac{1}{2\alpha} \left(\|F\|_{H^{-1}}^2 + \|h\|_{H^{-1/2}}^2 \right). \tag{29}$$

Now if $\mu = \mu(\theta)$ then

$$\begin{aligned} \int_{\Gamma_b} \bar{\mu} \frac{\langle D \rangle}{kb} \mu d\theta &= \int_{\Gamma_b} \left[\sum_{p=-\infty}^{\infty} \hat{\mu}_p e^{ip\theta} \right] \left[\sum_{p=-\infty}^{\infty} \frac{\langle p \rangle}{kb} \hat{\mu}_p e^{ip\theta} \right] d\theta = \int_{\Gamma_b} \sum_{p=-\infty}^{\infty} \left[\sum_{l=-\infty}^{\infty} \hat{\mu}_{p-l} \frac{\langle l \rangle}{kb} \hat{\mu}_l \right] e^{ip\theta} d\theta \\ &= \sum_{l=-\infty}^{\infty} \hat{\mu}_{-l} \frac{\langle l \rangle}{kb} \hat{\mu}_l = \sum_{l=-\infty}^{\infty} \bar{\hat{\mu}}_l \frac{\langle l \rangle}{kb} \hat{\mu}_l = \|\mu\|_{H^{1/2}}^2 \geq 0. \end{aligned} \tag{30}$$

Also,

$$\begin{aligned} \int_{\Gamma_b} \bar{\mu} R \mu d\theta &= \sum_{l=-\infty}^{\infty} \left[\hat{T}(l) + \frac{\langle l \rangle}{kb} \right] |\hat{\mu}_l|^2 \leq \sum_{l=-\infty}^{\infty} C |\hat{\mu}_l|^2 \leq \sum_{l=-\infty}^{\infty} C \left(\frac{1}{\beta \langle l \rangle} + \beta \langle l \rangle \right) |\hat{\mu}_l|^2 \\ &\leq \frac{C}{\beta} \|\mu\|_{H^{-1/2}}^2 + C\beta \|\mu\|_{H^{1/2}}^2. \end{aligned} \tag{31}$$

Using Eqs. (30) and (31), and

$$\|v_b\|_{H^{s-1/2}([0,2\pi])} \leq C \|v\|_{H^s(\Omega_{a,b})},$$

we can use (29) to deduce that

$$\left(1 - \frac{\alpha}{2} - C\beta\right) \|v\|_{H_0^1}^2 \leq \left(k^2 + \frac{C}{\beta}\right) \|v\|_{L^2}^2 + \frac{1}{2\alpha} \left(\|F\|_{H^{-1}}^2 + \|h\|_{H^{-1/2}}^2\right). \tag{32}$$

The uniqueness of the solution implies that the term involving the L^2 norm of v may be dropped from the right hand side (see [21], Section 6.2, Theorem 6), and the proof is complete once α and β are chosen sufficiently small. \square

The estimate which allows us to control the right hand side of (21) follows.

Lemma 5. *Let $s \geq 0$ be an integer and let $f \in C^{s+2}([0, 2\pi])$. Assume that*

$$\|u_n\|_{H^{s+2}(\Omega_{a,b})} \leq K_1 B^n \tag{33}$$

for all $n < N$ and constants K_1 and B . If

$$B > |f|_{C^{s+2}}, \tag{34}$$

there exists a C_0 such that

$$\|F_N\|_{H^s(\Omega_{a,b})} \leq K_1 |f|_{C^{s+2}} C_0 B^{N-1}, \tag{35a}$$

$$\|h_N\|_{H^{s+1/2}([0, 2\pi])} \leq K_1 |f|_{C^{s+2}} C_0 B^{N-1}. \tag{35b}$$

Proof. We begin with

$$\|F_N\|_{H^s} \leq \left\| \partial_r F_N^{(1)} \right\|_{H^s} + \left\| \partial_\theta F_N^{(2)} \right\|_{H^s} + \left\| F_N^{(3)} \right\|_{H^s}$$

from (22) and, for conciseness, consider the second term only; the other cases follow in an identical manner.

$$\begin{aligned} \left\| \partial_\theta F_N^{(2)} \right\|_{H^s} &\leq \left\| F_N^{(2)} \right\|_{H^{s+1}} \\ &\leq \left\| (\partial_{\theta'} f)(a-b)(b-r) \partial_r u_{N-1} \right\|_{H^{s+1}} + \|f \partial_\theta u_{N-1}\|_{H^{s+1}} \\ &\quad + \|f(\partial_\theta f)(b-r) \partial_r u_{N-2}\|_{H^{s+1}} + \|(a-b)f \partial_\theta u_{N-1}\|_{H^{s+1}} + \|f^2 \partial_\theta u_{N-2}\|_{H^{s+1}} \\ &\leq M|a-b|R|f|_{C^{s+2}} \|u_{N-1}\|_{H^{s+2}} + M|f|_{C^{s+1}} \|u_{N-1}\|_{H^{s+2}} \\ &\quad + M^2 R|f|_{C^{s+1}} |f|_{C^{s+2}} \|u_{N-2}\|_{H^{s+2}} + M|a-b| |f|_{C^{s+1}} \|u_{N-1}\|_{H^{s+2}} + M^2 |f|_{C^{s+1}}^2 \|u_{N-2}\|_{H^{s+2}} \\ &\leq K_1 |f|_{C^{s+2}} (C_0/3) B^{N-1}, \end{aligned}$$

where we have used

$$\|(b-r)u\|_{H^s} \leq R(s) \|u\|_{H^s},$$

provided that

$$B > |f|_{C^{s+2}}.$$

The calculation for h_N proceeds in a similar fashion.

$$\begin{aligned} \|h_N\|_{H^{s+1/2}} &\leq \left\| \frac{f}{a-b} T u_{N-1} \right\|_{H^{s+1/2}} \leq \frac{M}{|a-b|} |f|_{C^{s+1/2+\epsilon}} \|T u_{N-1}\|_{H^{s+1/2}} \leq \frac{M}{|a-b|} |f|_{C^{s+1/2+\epsilon}} C_T \|u_{N-1}\|_{H^{s+3/2}} \\ &\leq \frac{M C_T}{|a-b|} |f|_{C^{s+1/2+\epsilon}} C_t \|u_{N-1}\|_{H^{s+2}(\Omega_{a,b})} \leq K_1 |f|_{C^{s+2}} C_0 B^{N-1}, \end{aligned}$$

where C_T and C_t are bounding constants for the DNO and the trace operator respectively. \square

We are now in a position to prove Theorem 3.

Proof. (Theorem 3). The proof proceeds inductively and the case $n = 0$ follows directly from Lemma 4 with $F_0 \equiv 0$ and $h_0 \equiv 0$. We now assume that (24) holds for all $n < N$ and apply Lemma 4 which implies that

$$\|u_N\|_{H^{s+2}} \leq K_0 [\|F_N\|_{H^s} + \|h_N\|_{H^{s+1/2}}].$$

From Lemma 5, letting $K_1 = K_0 \|\xi\|_{H^{s+3/2}}$, we obtain

$$\|u_N\|_{H^{s+2}} \leq 2K_0 \{K_0 \|\xi\|_{H^{s+3/2}}\} |f|_{C^{s+2}} C_0 B^{N-1},$$

and (24) is established if $B > 2K_0 C_0 |f|_{C^{s+2}}$. \square

Remark 6. Based upon the result of Lemma 4 it would appear that the smoothness requirement of Theorem 3 could be improved from H^{s+2} to H^{s+1} ($s \geq 0$). If we briefly entertain this possibility and attempt the recursive proof outlined above we find that we must perform estimates (from $F_N^{(3)}$) of the form:

$$\|(a - b)fr\partial_r u_{N-1}\|_{H^{s-1}} \leq |a - b|R(s)M|f|_{C^{s-1}} \|u_{N-1}\|_{H^s},$$

which is valid, for f continuous, only if $s \geq 1$. This prohibits our current approach from gaining any more smoothness.

An important issue with regard to artificial boundary calculations is that of well-posedness. Grote and Keller [28] investigated this issue for the DtN-FE method in the case of zero boundary deformation and suggested a remedy: Replacing the non-local boundary condition at the artificial boundary with a combination of the DtN map and a low-order boundary condition which preserves well-posedness. For the case of the full DNO, $G(f)$, the same remedy works; the precise nature of the low-order boundary condition must be modified to accommodate the non-circular nature of \mathcal{B} . We note that our numerical simulations do not suffer from these “spurious eigenvalues.”

4. Numerical results

A number of problems of physical interest can be constructed to test the efficiency, accuracy, and robustness of the methods we propose. In this section we will focus on one such problem, computing the field generated by a point source. At the end of the section we will briefly present results on scattering from a star-shaped obstacle (see Fig. 8).

There are several parameters which characterize the calculations we have in mind. Our numerics were carried out in MATLAB and the command “initmesh” was used with parameter h_{Max} (an estimate of the mesh parameter h , c.f. (7)) to triangulate the domain. We use piecewise linear basis functions in our FEM, so in order to evaluate the matrix Q , (9c), we must apply the DNO to piecewise linear functions at the boundary \mathcal{B} . As we have seen from formulas (16) and (18), the G_n are most naturally computed for functions expressed as Fourier series. While most of the boundary perturbations, f , we consider have only a finite number of Fourier coefficients, the piecewise linear Dirichlet data, ξ , have an infinite number and must be truncated; the parameter N_ξ expresses the number of Fourier coefficients we retain in ξ , i.e. we approximate ξ by

$$\xi_{N_\xi}(\theta) = \sum_{p=-N_\xi}^{N_\xi} \hat{\xi}_p e^{ip\theta} \tag{36}$$

where $\hat{\xi}_p$ are the Fourier coefficients of ξ . In a similar fashion we approximate f by the finite Fourier series

$$f_{N_f}(\theta) = \sum_{p=-N_f}^{N_f} \hat{f}_p e^{ip\theta} \tag{37}$$

where \hat{f}_p are the Fourier coefficients of f . As we mentioned above, often the f that we choose contain only a finite number of non-zero Fourier coefficients so that if N_f is chosen large enough an exact representation is achieved.

We have found that it is *crucial* for optimal performance of our algorithm that the $\hat{\xi}_p$ and \hat{f}_p be computed accurately. In response to this we have programmed either the *exact* Fourier coefficients (when they are convenient) or else used high-order quadratures to approximate them. In the case of the boundary “hat-function” supported on $[a, b] \cup [b, c]$,

$$\xi(\theta) = \begin{cases} (\theta - a)/(b - a) & a \leq \theta < b, \\ (\theta - c)/(b - c) & b \leq \theta < c, \\ 0 & \text{else,} \end{cases}$$

these coefficients are

$$\hat{\xi}_p = \frac{(b - c)e^{-iap} + (c - a)e^{-ibp} + (a - b)e^{-icp}}{2\pi(a - b)(b - c)p^2},$$

for $p \neq 0$, and $\hat{\xi}_0 = (c - a)/(4\pi)$. The performance of the OE and FE algorithms depend strongly on the smoothness properties of both the boundary deformation f and the Dirichlet data ξ . As more terms are used in the expansion of the DNO, convolution products cause information to move to higher and higher wavenumbers, and, unless this information is retained, the errors due to aliasing and the ill-conditioning in the OE and FE algorithms become overwhelming [46–48]. The vectors holding the Fourier coefficients of f and ξ are taken to be of length N_θ so that wavenumbers $-N_\theta/2, \dots, N_\theta/2 - 1$ can be represented. In order to completely avoid aliasing effects at order j a quick inspection of the OE and FE formulas reveals that

$$N_\theta/2 - 1 \geq jN_f + N_\xi,$$

or

$$N_\theta \geq 2jN_f + 2N_\xi + 2.$$

Finally, the parameter N_{DNO} specifies the number of terms G_n retained in the Taylor expansion of the DNO, and δ measures the size of the perturbation from the canonical geometry.

4.1. Point source problem

An exact, *point source* solution of the two dimensional problem

$$\Delta v + k^2 v = -\delta(x - x_0) \quad \text{in } \mathbf{R}^2 \tag{38a}$$

$$\lim_{r \rightarrow \infty} r^{1/2}(\partial_r v - ikv) = 0, \tag{38b}$$

is given by [44]

$$v_{\text{ps}}(x) = \frac{i}{4} H_0^{(1)}(k|x - x_0|) \tag{39}$$

for any $x_0 \in \mathbf{R}^2$. Upon insertion of an artificial boundary $\mathcal{B} = \{r = a + \delta f\}$, (38) is equivalent to

$$\Delta v + k^2 v = -\delta(x - x_0) \quad r < a + \delta f \tag{40a}$$

$$\nabla v \cdot N_{\delta f} = G(\delta f)v \quad \text{at } r = a + \delta f. \tag{40b}$$

Therefore, a simple test of the utility of our approach is to compare the exact solution v_{ps} to the numerical solution of (40) via the FEM on $\{r < a + \delta f\}$ with the DNO implemented using the FE and OE methods. Of course (40) and (5) are quite different problems so a modification of the FEM is required and, rather than solving the linear system (8), we solve the modified system

$$(-K + k^2 M + Q)\vec{v} = \vec{F}$$

with K , M , and Q given in (9) (replace $\Omega(\Sigma, \mathcal{B})$ by $\{r < a + \delta f\}$), and

$$\vec{F}_k = - \int_{r < a + \delta f} \delta(x - x_0) \varphi_k \, dV.$$

To illustrate the behavior of our method we have selected $x_0 = (0, 0)$, $a = 1$, $k = 11/8$,

$$f(\theta) = \cos(4\theta),$$

and $\delta = 0, 1/100, 1/10$. In each of these cases we display results of a sequence of simulations with h_{Max} ranging over two orders of magnitude:

$$h_{\text{Max}} = 10^j \quad j = 0, -1/2, -1, -3/2, -2. \tag{41}$$

The relative L^∞ errors at the boundary, when compared with the solution (39), for our method with the DNO implemented via OE and FE are computed. In addition we present results for a third method, the ‘‘control FEM,’’ which is the piecewise linear FEM applied to the problem

$$\Delta v + k^2 v = -\delta(|x|) \quad r < a + \delta f, \tag{42a}$$

$$v(a + \delta f, \theta) = H_0^{(1)}(k|a + \delta f|) \quad \text{at } r = a + \delta f, \tag{42b}$$

i.e. we have supplied the *exact* Dirichlet data at the outer boundary from the exact solution (39). While this problem is unrealistic it is instructive to compare our method to an idealized one which contains errors due to the FEM discretization alone.

We begin with the case $\delta = 0$ which corresponds to the method of Keller et al. ($G(f) = G_0$ and $G_n(f) = 0$ for $n > 0$). In Fig. 2(a) we show the triangulation of the computational domain when $h_{\text{Max}} = 1/10$, and in Fig. 2(b) we display the errors when computing with the control FEM, OE, and FE methods with $\delta = 0$, $N_{\text{DNO}} = 0$, $N_\theta = 4$, $N_\xi = 1$, and $N_f = 4$.

In our next experiment we investigate the behavior of our method for a perturbation of small size, $\delta = 1/100$. In Fig. 3(a) we show the triangulation of the computational domain when $h_{\text{Max}} = 1/10$, and in Fig. 3(b) we display the errors when computing with the control FEM, OE, and FE methods with $\delta = 1/100$, $N_{\text{DNO}} = 2$, $N_\theta = 16$, $N_\xi = 4$, and $N_f = 4$.

We now consider a perturbation of moderate size, $\delta = 1/10$. In Fig. 4(a) we show the triangulation of the computational domain when $h_{\text{Max}} = 1/10$, and in Fig. 4(b) we display the errors when computing with the control FEM, OE, and FE methods with $\delta = 1/10$, $N_{\text{DNO}} = 8$, $N_\theta = 64$, $N_\xi = 8$, and $N_f = 4$.

Finally, for each of the problems, the error data was fit using least-squares, to a power law,

$$e = C(h_{\text{Max}})^p, \tag{43}$$

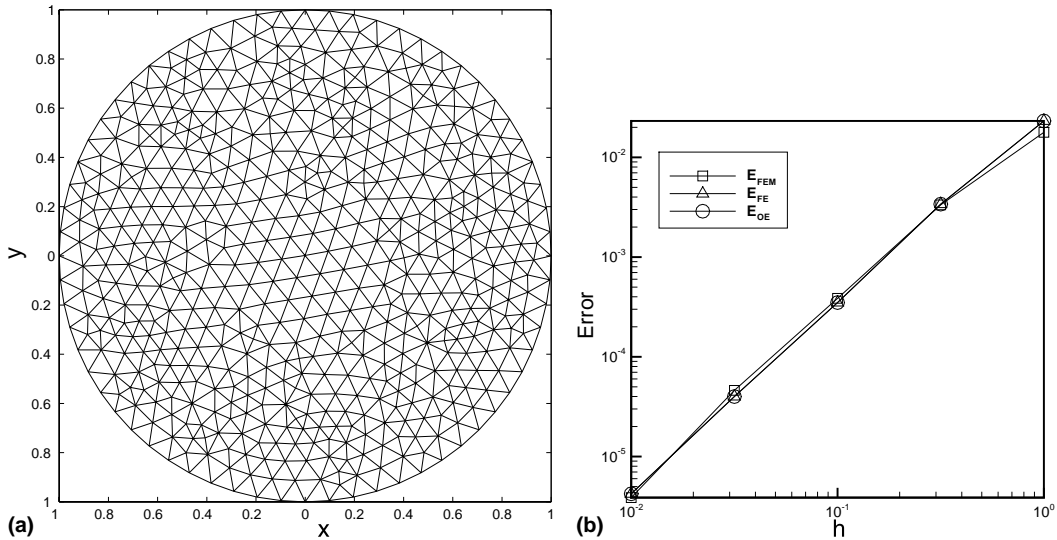


Fig. 2. Plots of computational domain and L^∞ error versus h for zero perturbation, $\delta = 0$; $N_{\text{DNO}} = 0$, $N_\theta = 4$, $N_\xi = 1$, and $N_f = 4$. (a) Domain triangulation ($\delta = 0$); (b) Plot of L^∞ error versus h .

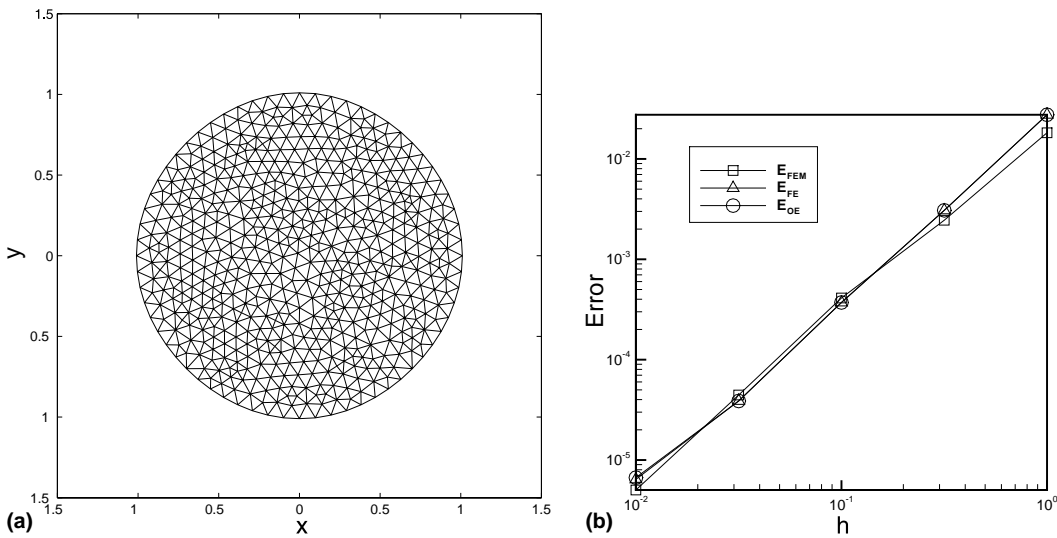


Fig. 3. Plots of computational domain and L^∞ error versus h for small perturbation, $\delta = 1/100$; $N_{\text{DNO}} = 2$, $N_\theta = 16$, $N_\xi = 4$, and $N_f = 4$. (a) Domain triangulation ($\delta = 1/100$); (b) Plot of L^∞ error versus h .

where p should be roughly two for errors due solely to the piecewise linear finite element discretization. The results are summarized in Table 1 for all three experiments discussed above. We note that for a deformation of size zero the solution’s angular homogeneity indicates that a small number of Fourier coefficients, N_ξ and N_θ , are necessary while, of course, N_{DNO} may be set to zero. For $\delta > 0$ this homogeneity is broken so more Fourier coefficients are necessary to accurately represent ξ , while increasing δ requires more terms N_{DNO} in the series for the DNO. For instance, the results for $\delta = 1/10$ were significantly worse if N_{DNO} were set to 4 or 6.

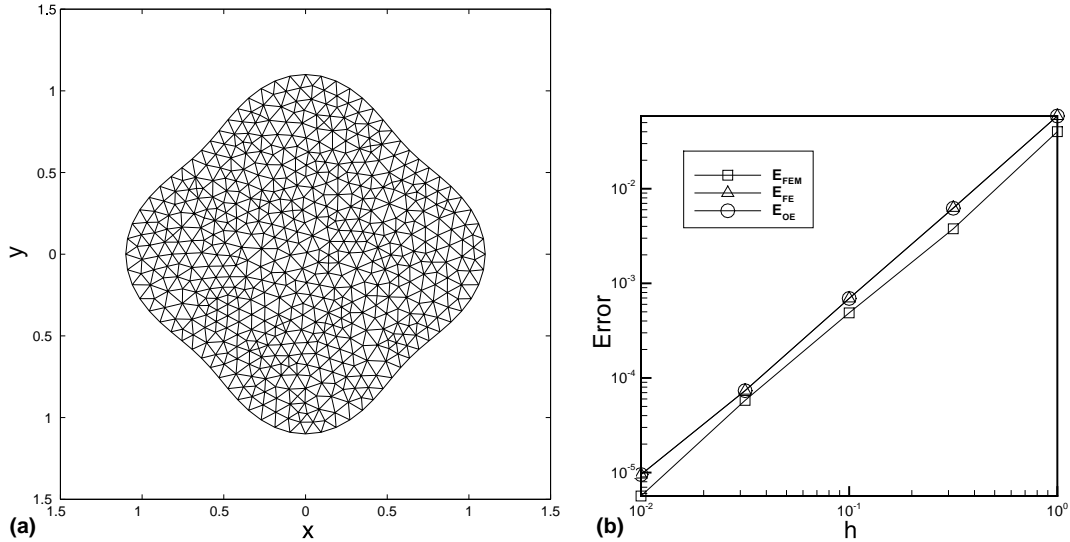


Fig. 4. Plots of computational domain and L^∞ error versus h for moderate perturbation, $\delta = 1/10$; $N_{\text{DNO}} = 8$, $N_\theta = 64$, $N_\xi = 8$, and $N_f = 4$. (a) Domain triangulation ($\delta = 1/10$); (b) Plot of L^∞ error versus h .

Table 1
Point source: rate of convergence exponents p (see (43)) for control FEM, OE, and FE

δ	N_{DNO}	N_θ	N_ξ	N_f	Control FEM	OE	FE
0	0	4	1	4	1.84	1.88	1.88
1/100	2	16	4	4	1.77	1.83	1.83
1/10	8	64	8	4	1.90	1.90	1.90

To consider deformations of large size we have found it necessary to incorporate techniques of analytic continuation in the computation of the DNO which are justified in Theorem 2. The technique we choose, based upon the success in [48], is Padé approximation and it is implemented in the following way: Both the OE and FE methods for approximating the DNO to order N_{DNO} can be expressed as

$$\begin{aligned}
 G^{N_{\text{DNO}}}(\delta f)\xi &= \sum_{n=0}^{N_{\text{DNO}}} (G_n(f)\xi)\delta^n = \sum_{n=0}^{N_{\text{DNO}}} \left(\sum_{p=-\infty}^{\infty} a_{n,p} e^{ip\theta} \right) \delta^n = \sum_{p=-\infty}^{\infty} \left(\sum_{n=0}^{N_{\text{DNO}}} a_{n,p} \delta^n \right) e^{ip\theta} \\
 &= \sum_{p=-\infty}^{\infty} S_p^{N_{\text{DNO}}}(\delta) e^{ip\theta},
 \end{aligned} \tag{44}$$

where $S_p^{N_{\text{DNO}}}$ is a polynomial of degree N_{DNO} in δ . We approximate $S_p^{N_{\text{DNO}}}$ by the unique rational function (Padé approximant) of degree L over M accurate to order $L + M + 1$ [2]. In all experiments conducted N_{DNO} was even so only diagonal approximants were considered, i.e. $L = M = N_{\text{DNO}}/2$. Padé approximants have some amazing properties of approximation of (a large subclass of) analytic functions from their Taylor series for points far outside their radii of convergence, see e.g. [2]. A linear set of equations for the denominator coefficients, and simple formulas for the numerator coefficients allow for their straightforward calculation.

With this technique in place, we now pursue a large deformation of the base (circular) geometry corresponding to $\delta = 1/3$. In Fig. 5(a) we show the triangulation of the computational domain when

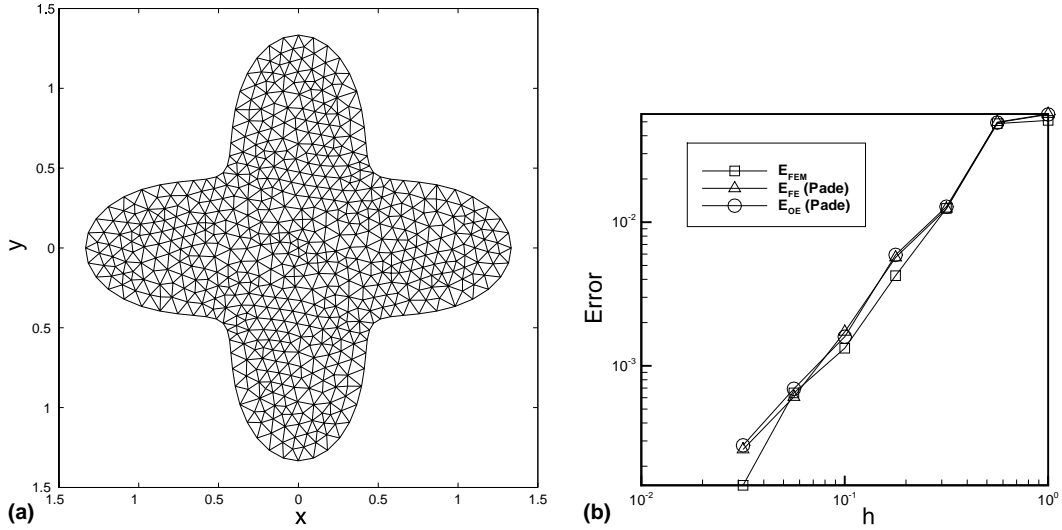


Fig. 5. Plots of computational domain and L^∞ error versus h for large perturbation, $\delta = 1/3$; $N_{DNO} = 16$, $N_\theta = 128$, $N_\xi = 8$, and $N_f = 4$. (a) Domain triangulation ($\delta = 1/3$); (b) Plot of L^∞ error versus h .

$h_{Max} = 1/10$, and in Fig. 5(b) we display the errors when computing with the control FEM, OE (Padé), and FE (Padé) methods with $\delta = 1/3$, $N_{DNO} = 16$, $N_\theta = 128$, $N_\xi = 8$, and $N_f = 4$.

In this set of runs the set of h_{Max} was restricted to one and a half orders of magnitude,

$$h_{Max} = 10^j \quad j = 0, -1/2, -1, -3/2.$$

We found that the results for $h_{Max} = 1/100$, while continuing to provide increased accuracy, did not provide an order two improvement. We suspect, based upon preliminary investigations left for future work, that the matrix Q becomes ill-conditioned at a somewhat faster rate than K or M as h is refined for N_{DNO} large. Despite this, note that while the OE and FE methods provide inaccurate answers throughout all orders of h_{Max} , if Padé approximation is added to the algorithm, orders of accuracy $p_{OE} = 1.67$ and $p_{FE} = 1.65$, as compared to $p_{FEM} = 1.76$, can be achieved. This clearly demonstrates the fact $\delta = 1/3$ is *outside* the disk of convergence of the DNO assured by Theorem 1 while being *inside* the region of extended analyticity guaranteed by Theorem 2. Furthermore, only through techniques of analytic continuation, such as Padé approximation, can these regions of extended analyticity be accessed.

As a final pair of tests within the point source context we would like to display how two other important artificial boundary shapes can be easily implemented within our framework. We consider boundaries shaped as an ellipse with major and minor axes a and b ,

$$\rho_e(\theta) = \frac{ab}{\sqrt{b^2 \cos^2(\theta) + a^2 \sin^2(\theta)}},$$

and a rectangle of side lengths $2a$ and $2b$,

$$\rho_r(\theta) = \begin{cases} a/\cos(\theta) & 0 \leq \theta < \theta^* \\ b/\sin(\theta) & \theta^* \leq \theta < \pi - \theta^* \\ a/\cos(\theta) & \pi - \theta^* \leq \theta < \pi + \theta^* \\ b/\sin(\theta) & \pi + \theta^* \leq \theta < 2\pi - \theta^* \\ a/\cos(\theta) & 2\pi - \theta^* \leq \theta < 2\pi, \end{cases}$$

where $\theta^* = a \tan^{-1}(b/a)$. It should be noted that since these shapes each possess an infinite number of non-zero Fourier coefficients, when we truncate their Fourier series representations at wavenumber N_f the resulting shapes will be only approximate ellipses and rectangles. Of course, we may make them as close as we like to ellipses and rectangles, respectively, by increasing N_f .

For the elliptically shaped boundary we selected $a = 1.25$ and $b = 1/1.25$, and discovered that with $N_{\text{DNO}} = 8$, $N_\theta = 128$, $N_\xi = 8$ and $N_f = 8$ we could, without Padé enhancement, achieve rates of convergence $p_{\text{OE}} = 1.81$ and $p_{\text{FE}} = 1.81$ while $p_{\text{FEM}} = 1.98$. A picture of the triangulation of the computational domain when $h_{\text{Max}} = 1/10$ is given in Fig. 6(a), while Fig. 6(b) displays the errors when computing with the control FEM, OE, and FE methods.

For the rectangular shaped boundary we selected $a = 1.1$ and $b = 1/1.1$, and we discovered that with $N_{\text{DNO}} = 12$, $N_\theta = 256$, $N_\xi = 16$ and $N_f = 16$ we could, with Padé enhancement, achieve rates of convergence $p_{\text{OE}} = 1.80$ and $p_{\text{FE}} = 1.83$ while $p_{\text{FEM}} = 1.92$. A picture of the triangulation of the computational domain when $h_{\text{Max}} = 1/10$ is given in Fig. 7(a), while Fig. 7(b) displays the errors when computing with the control FEM, OE, and FE methods.

4.2. Irregular obstacle scattering

We conclude our experiments by returning to the obstacle scattering problem (5) with a star-shaped scatterer (see Fig. 8) which we specify by the equation

$$\Sigma = \{(r, \theta) | r \leq 1 + 0.4 \cos(4\theta)\}.$$

We enclose this with an artificial boundary \mathcal{B} of the form $\{r = a + \delta \cos(4\theta)\}$ and report results for $a = 1.5$ and $\delta = 0.3$ (see Fig. 8(a)), which represents a large (20%) deformation of the base (circular) geometry. Of course an analytical solution is no longer available so we compare our results with a highly resolved zero-deformation DtN-FE computation [37] with artificial boundary at the circle, $r = 1.8$. This radius is chosen as it both encloses the obstacle, and maintains the same minimum distance to the scatterer as our new approach (see Fig. 8(b)).

We now present a comparison, in the L^∞ norm at the surface of the scatterer Γ_Σ , of the (scattered) field computed via our method (OE implementation with Padé summation) with the highly resolved zero-deformation DtN-FE computation. The domain is depicted in Fig. 9(a) and the error (in L^∞ norm at the boundary) as h_{Max} is refined is displayed in Fig. 9(b). These numerical runs were conducted with the

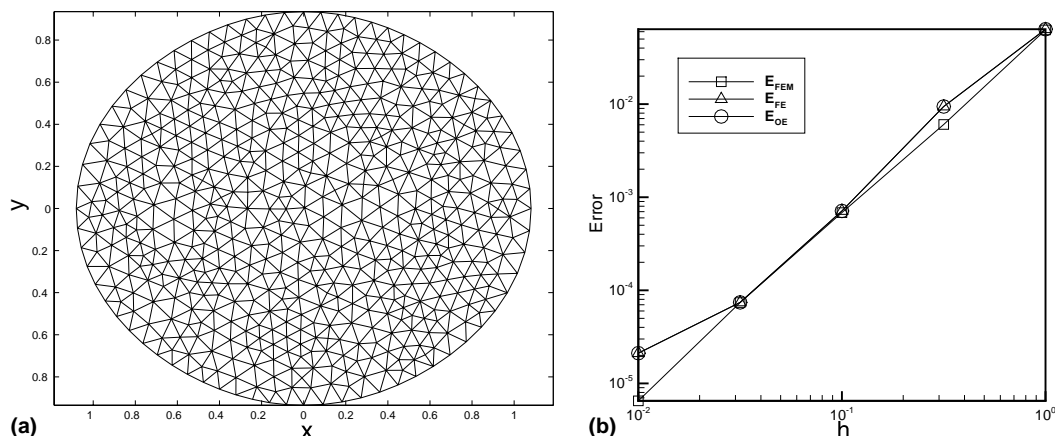


Fig. 6. Plots of computational domain and L^∞ error versus h for elliptical boundary; $N_{\text{DNO}} = 8$, $N_\theta = 128$, $N_\xi = 8$, and $N_f = 8$. (a) Domain triangulation (ellipse); (b) Plot of L^∞ error versus h .

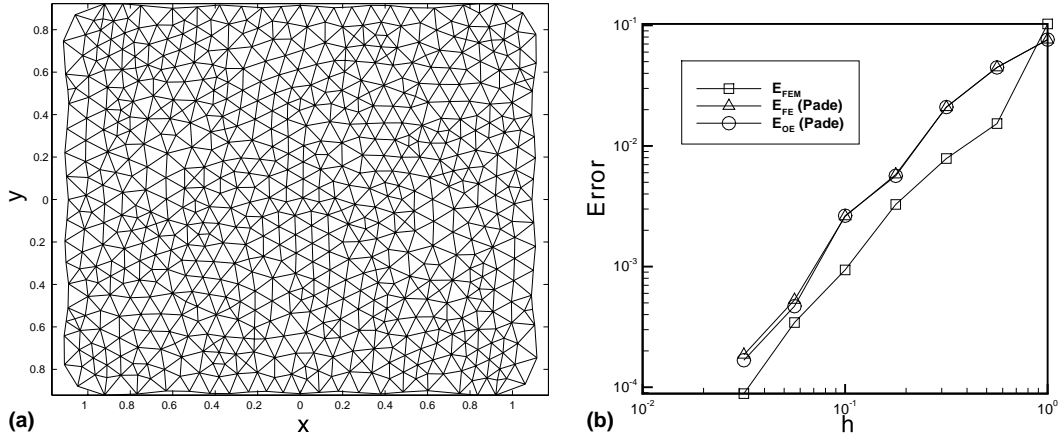


Fig. 7. Plots of computational domain and L^∞ error versus h for rectangular boundary; $N_{\text{DNO}} = 12$, $N_\theta = 256$, $N_\xi = 16$, and $N_f = 16$. (a) Domain triangulation (rectangle); (b) Plot of L^∞ error versus h .

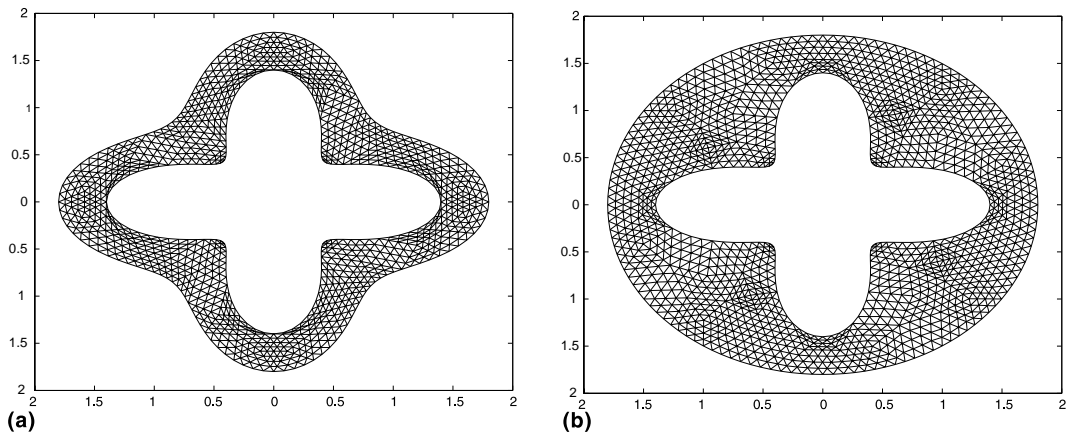


Fig. 8. Plots of computational domain using star-shaped and circular artificial boundary. (a) Domain triangulation using star-shaped boundary: $\Sigma = \{r = 1.5 + 0.3 \cos(4\theta)\}$; (b) Domain triangulation using circular boundary: $\Sigma = \{r = 1.8\}$.

parameter values $N_{\text{DNO}} = 8$, $N_\theta = 84$, $N_\xi = 8$, and $N_f = 4$. The convergence results are also summarized in Table 2 and a least squares fit to the power law (43) reveals a rate of convergence $p = 1.77$ indicating that the errors are dominated by those of the underlying FEM.

This computation shows that our new method can be used to advantage in realistic scattering computations. Clearly, the simulation using the perturbative DNO converges stably to the zero-deformation DtN-FE calculation, while using far fewer elements. In particular, at each refinement level the number of triangles, N_t (star), in the star-shaped geometry is roughly 3/4 that of the number, N_t (zero), required by a circular geometry of radius 1.8; see Fig. 8. We note that for the star-shaped scatterer chosen for this computation an ellipsoidal artificial boundary would provide no computational advantage (in terms of number of triangles required) over the circular boundary; a perturbation of general form is required for significant computational savings.

The convergence study above confirms that our method converges to the *true* solution, however, in a realistic scattering computation the strategy is to implement one algorithm on a sequence of refined meshes,

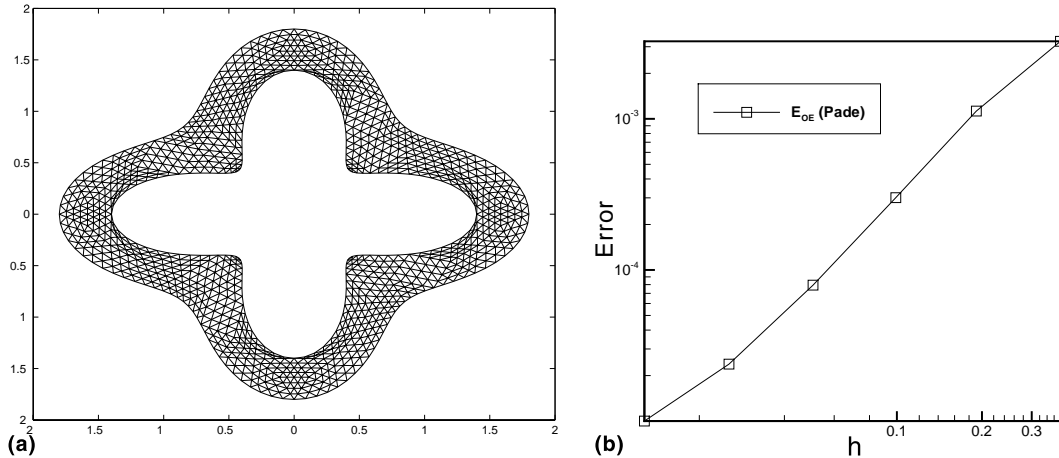


Fig. 9. Plots of computational domain and L^∞ error versus h for star-shaped boundary; $N_{\text{DNO}} = 8$, $N_\theta = 84$, $N_\xi = 8$, and $N_f = 4$. (a) Domain triangulation (airplane scatterer); (b) Plot of L^∞ error versus h .

Table 2

Star-shaped scatterer: L^∞ errors for DtN-FE method with star-shaped boundary on scatterer surface, compared to highly resolved computation using circular (zero-deformation) boundary

Refinement level	h_{Max}	N_t (star)	N_t (zero)	L^∞ error
0	0.3791	128	168	3.25×10^{-3}
1	0.1911	512	672	1.13×10^{-3}
2	0.0991	2048	2688	3.01×10^{-4}
3	0.0505	8192	10,752	7.93×10^{-5}
4	0.0255	32,768	43,008	2.38×10^{-5}
5	0.0128	131,072	172,032	1.00×10^{-5}

Also listed are the number of triangles, N_t (star), at each level of refinement and, for comparison, the number of triangles, N_t (zero), which a zero-deformation computation would require.

Table 3

Star-shaped scatterer: L^2 errors for DtN-FE method with star-shaped boundary on scatterer surface, compared to highly resolved computation

Refinement level	h_{Max}	N_t (star)	L^2 error
0	0.3791	128	5.46×10^{-2}
1	0.1911	512	1.72×10^{-2}
2	0.0991	2048	4.68×10^{-3}
3	0.0505	8192	1.17×10^{-3}
4	0.0255	32,768	2.46×10^{-4}

and compare (in the L^2 norm) the solution at each level of refinement with the finest-mesh calculation. We present such an error analysis with the parameter values as above ($N_{\text{DNO}} = 8$, $N_\theta = 84$, $N_\xi = 8$, and $N_f = 4$) and the DNO implemented via the OE algorithm with Padé summation. The computational region is $\Omega(\Sigma, \mathcal{B})$ (see Fig. 9(a)), and the errors are reported in the L^2 norm over this region, with reference to the fine-grid computation. The convergence results are summarized in Table 3. A least squares fit to the power law (43) reveals a rate of convergence $p = 2.02$, in accordance with that expected for ordinary FEM.

In future research we aim to extend this method to the three dimensional Helmholtz problem (acoustic scattering) and the full set of three dimensional Maxwell's equations. While the implementation details of the DNO in this setting will be somewhat different (complex exponentials and Hankel functions must be replaced by spherical harmonics and spherical Hankel functions), the FEM framework will be largely the same.

Acknowledgements

The authors wish to thank Fernando Reitich for suggesting this problem and helpful discussions. DPN gratefully acknowledges support from NSF through grants No. DMS-0196452 and DMS-0139822. NN gratefully acknowledges support from NSERC through grant G202886. A portion of this work was conducted during a visit to the Institute for Mathematics and Its Applications (University of Minnesota) whose supportive research environment the authors gratefully acknowledge.

References

- [1] S. Arbabanel, D. Gottlieb, J.S. Hesthaven, Long-time behaviour of the perfectly matched layer equations in computational electromagnetics, *J. Sci. Comput.* 17 (2002) 405–422.
- [2] G.A. Baker Jr., P.G. Morris, *Padé Approximants*, second ed., Cambridge University Press, Cambridge, 1996.
- [3] E. Bécache, P. Joly, On the analysis of Bérenger's perfectly matched layers for Maxwell's equations, *Math. Model. Numer. Anal.* 36 (2002) 87–119.
- [4] J.-P. Bérenger, A perfectly matched layer for the absorption of electromagnetic waves, *J. Comput. Phys.* 114 (1994) 185–200.
- [5] O.P. Bruno, F. Reitich, Solution of a boundary value problem for the Helmholtz equation via variation of the boundary into the complex domain, *Proc. Roy. Soc. Edinburgh Sect. A* 122 (3–4) (1992) 317–340.
- [6] O.P. Bruno, F. Reitich, Numerical solution of diffraction problems: a method of variation of boundaries, *J. Opt. Soc. Am. A* 10 (6) (1993) 1168–1175.
- [7] O.P. Bruno, F. Reitich, Numerical solution of diffraction problems: a method of variation of boundaries. ii. Finitely conducting gratings, Padé approximants, and singularities, *J. Opt. Soc. Am. A* 10 (11) (1993) 2307–2316.
- [8] O.P. Bruno, F. Reitich, Numerical solution of diffraction problems: a method of variation of boundaries. iii. Doubly periodic gratings, *J. Opt. Soc. Am. A* 10 (12) (1993) 2551–2562.
- [9] O.P. Bruno, F. Reitich, Approximation of analytic functions: a method of enhanced convergence, *Math. Comp.* 63 (207) (1994) 195–213.
- [10] O.P. Bruno, F. Reitich, Calculation of electromagnetic scattering via boundary variations and analytic continuation, *Appl. Comput. Electromag. Soc. J.* 11 (1) (1996) 17–31.
- [11] O.P. Bruno, F. Reitich, Boundary-variation solutions for bounded-obstacle scattering problems in three dimensions, *J. Acoust. Soc. Am.* 104 (5) (1998) 2579–2583.
- [12] O.P. Bruno, F. Reitich, High-order boundary perturbation methods, in: *Mathematical Modeling in Optical Science*, Frontiers in Applied Mathematics Series, SIAM, 1999.
- [13] A.P. Calderón, Cauchy integrals on Lipschitz curves and related operators, *Proc. Nat. Acad. Sci. USA* 75 (1977) 1324–1327.
- [14] D. Colton, R. Kress, *Inverse Acoustic and Electromagnetic Scattering Theory*, second ed., Springer-Verlag, Berlin, 1998.
- [15] R. Coifman, Y. Meyer, Nonlinear harmonic analysis and analytic dependence, in: *Pseudodifferential Operators and Applications*, American Mathematical Society, Providence, RI, 1985, pp. 71–78.
- [16] W. Craig, D.P. Nicholls, Traveling two and three dimensional capillary gravity water waves, *SIAM J. Math. Anal.* 32 (2) (2000) 323–359.
- [17] W. Craig, C. Sulem, Numerical simulation of gravity waves, *J. Computat. Phys.* 108 (1993) 73–83.
- [18] W. Craig, U. Schanz, C. Sulem, The modulation regime of three-dimensional water waves and the Davey–Stewartson system, *Ann. Inst. Henri Poincaré* 14 (1997) 615–667.
- [19] R. Djellouli, C. Farhat, A. Macedo, R. Tezaur, Finite element solution of two-dimensional acoustic scattering problems using arbitrarily shaped convex artificial boundaries, *J. Comp. Acoustics* 8 (2000) 81–99.
- [20] D.G. Dommermuth, D.K.P. Yue, A high-order spectral method for the study of nonlinear gravity waves, *J. Fluid Mech.* 184 (1987) 267–288.
- [21] L.C. Evans, *Partial Differential Equations*, American Mathematical Society, Providence, RI, 1998.

- [22] D. Givoli, Nonreflecting boundary conditions, *J. Comput. Phys.* 94 (1) (1991) 1–29.
- [23] D. Givoli, Numerical methods for problems in infinite domains, *Studies in Applied Mechanics*, vol. 33, Elsevier Scientific Publishing, Amsterdam, 1992.
- [24] D. Givoli, Recent advances in the DtN-FE method, *Arch. Comput. Methods Eng.* 6 (2) (1999) 71–116.
- [25] D. Givoli, Scattering matrix of a nearly circular cylinder, *Wave Motion* 30 (3) (1999) 239–251.
- [26] D. Givoli, J.B. Keller, Special finite elements for use with high-order boundary conditions, *Comput. Methods Appl. Mech. Eng.* 119 (3–4) (1994) 199–213.
- [27] M.J. Grote, J.B. Keller, Exact nonreflecting boundary conditions for the time dependent wave equation, *SIAM J. Appl. Math.* 55 (2) (1995) 280–297.
- [28] M.J. Grote, J.B. Keller, On nonreflecting boundary conditions, *J. Comput. Phys.* 122 (2) (1995) 231–243.
- [29] M.J. Grote, J.B. Keller, Nonreflecting boundary conditions for time-dependent scattering, *J. Comput. Phys.* 127 (1) (1996) 52–65.
- [30] M.J. Grote, J.B. Keller, Nonreflecting boundary conditions for Maxwell's equations, *J. Comput. Phys.* 139 (2) (1998) 327–342.
- [31] D. Gilbarg, N.S. Trudinger, *Elliptic Partial Differential Equations of Second Order*, second ed., Springer-Verlag, Berlin, 1983.
- [32] H.D. Han, X.N. Wu, Approximation of infinite boundary condition and its application to finite element methods, *J. Comp. Math.* 3 (1985) 2.
- [33] L. Hörmander, Pseudo-differential operators and non-elliptic boundary problems, *Ann. Math.* (2) (1966) 83.
- [34] G.C. Hsiao, W. Wendland, A finite element method for some integral equations of the first kind, *J. Math. Anal. Appl.* 58 (1977) 449–481.
- [35] C. Johnson, J.-C. Nédélec, On the coupling of boundary integral and finite element methods, *Math. Comp.* 35 (1980) 1063–1079.
- [36] C. Johnson, *Numerical Solution of Partial Differential Equations by the Finite Element Method*, Cambridge University Press, Cambridge, 1987.
- [37] J.B. Keller, D. Givoli, Exact nonreflecting boundary conditions, *J. Comput. Phys.* 82 (1) (1989) 172–192.
- [38] O.A. Ladyzhenskaya, N.N. Ural'tseva, *Linear and Quasilinear Elliptic Equations*, Academic Press, New York, 1968.
- [39] D.M. Milder, An improved formalism for rough-surface scattering of acoustic and electromagnetic waves, in: *Proceedings of SPIE – The Inter. Soc. for Opt. Eng.*, San Diego, 1991, vol. 1558, *Int. Soc. Opt. Eng.*, Bellingham, WA, 1991, pp. 213–221.
- [40] D.M. Milder, An improved formalism for wave scattering from rough surfaces, *J. Acoust. Soc. Am.* 89 (2) (1991) 529–541.
- [41] D.M. Milder, An improved formalism for electromagnetic scattering from a perfectly conducting rough surface, *Radio Sci.* 31 (6) (1996) 1369–1376.
- [42] D.M. Milder, Role of the admittance operator in rough-surface scattering, *J. Acoust. Soc. Am.* 100 (2) (1996) 759–768.
- [43] D.M. Milder, H.T. Sharp, An improved formalism for rough surface scattering. ii. Numerical trials in three dimensions, *J. Acoust. Soc. Am.* 91 (5) (1992) 2620–2626.
- [44] J.-C. Nédélec, *Acoustic and Electromagnetic Equations*, Springer-Verlag, New York, 2001.
- [45] D.P. Nicholls, *Traveling Gravity Water Waves in Two and Three Dimensions*, PhD thesis, Brown University, 1998.
- [46] D.P. Nicholls, F. Reitich, A new approach to analyticity of Dirichlet–Neumann operators, *Proc. Roy. Soc. Edinburgh Sect. A* 131 (6) (2001) 1411–1433.
- [47] D.P. Nicholls, F. Reitich, Stability of high-order perturbative methods for the computation of Dirichlet–Neumann operators, *J. Comp. Phys.* 170 (1) (2001) 276–298.
- [48] D.P. Nicholls, F. Reitich, Analytic continuation of Dirichlet–Neumann operators, *Numer. Math.* 94 (1) (2003) 107–146.
- [49] R. Petit (Ed.), *Electromagnetic Theory of Gratings*, Springer-Verlag, Berlin, 1980.
- [50] V.S. Ryaben'kii, Difference potentials method and its applications, *Math. Nachr.* 177 (1996) 251–264.
- [51] R. Seeley, Topics in pseudo-differential operators, *Pseudo-Diff. Operators (C.I.M.E., Stresa, 1968)*, 1969, pp. 167–305.
- [52] S.V. Tsynkov, Numerical solution of problems on unbounded domains. A review, *Appl. Numer. Math.* 27 (4) (1998) 465–532.
- [53] C. Yeh, Perturbation approach to the diffraction of electromagnetic waves by arbitrarily shaped dielectric obstacles, *Phys. Rev.* 135 (5A) (1964) 1193–1201.
- [54] V. Zakharov, Stability of periodic waves of finite amplitude on the surface of a deep fluid, *J. Appl. Mech. Tech. Phys.* 9 (1968) 190–194.